

Accurate Parameter Estimation of Quadratic Curves from Grey-Level Images

R. SAFAEE-RAD,* I. TCHOUKANOV,† B. BENHABIB,* AND K. C. SMITH*†‡

*Computer Integrated Manufacturing Laboratory and Departments of *Mechanical Engineering, †Electrical Engineering, and ‡Computer Science, University of Toronto, 5 King's College Road, Toronto, Ontario, Canada M5S 1A4*

Received November 29, 1990; accepted January 9, 1991

Accurate estimation of the parameters of a curve present in a grey-level image is required in various machine-vision and computer-vision problems. Quadratic curves are more common than other curve types in these fields. The accuracy of the estimated parameters depends not only on the global interpolation technique used, but, as well, on compensation of major sources of error. In this paper, first, as a preliminary step in accurate parameter estimation of quadratic curves, a sequential distortion-compensation procedure is formulated. This procedure addresses the major distortion factors involved in the transformation of a curve from the object space to the image space. Subsequently, as a means for accurate estimation of the coordinates of edge points, a new sub-pixel edge detector based on the principle of the sample-moment-preserving transform (SMPT) is developed. A circular-arc geometry is assumed for the boundary inside the detection area. The new arc-edge detector is designed as a cascade process using a linear-edge detector and a look-up table. Its performance is compared with that of a linear subpixel edge detector. Then, as a part of the main theme of the paper, the estimation of the five basic parameters of an elliptical shape based on its edge-point data is addressed. To achieve the desired degree of accuracy, a new error function is introduced, and as the basis for a comparative study, an objective and independent measure for "goodness" of fit is derived. The proposed new error function and two other error functions previously developed are applied to six different situations. The comparative performance of these error functions is discussed. Finally, as the basis for evaluation of the total process, a 3D location estimation problem is considered. The objective is to accurately estimate the orientation and position in 3D of a set of circular features. The experimental results obtained are significant in two separate ways: in general, they show the validity of the overall process introduced here in the accurate estimation of 3D location; in particular, they demonstrate the effectiveness of the sub-pixel edge detector and the global interpolation technique, both developed here. © 1991 Academic Press, Inc.

1. INTRODUCTION

Estimation of the parameters of a curve from a grey-level image is required in various situations in machine vision. Depending on the required level of accuracy and the conditions under which the estimation is to be carried

out, various combinations of external factors must be taken into account. For example, in some cases, a process of simple global thresholding and simple global curve fitting may suffice without considering various sources of errors inherent in the transformation from object space into image space. Clearly, however, this simple approach does not yield very accurate estimation of a curve's parameters.

In this paper, we present a generally applicable practical method for accurate estimation of parameters of curves represented by grey-level images. The method considers not only an accurate global interpolation process, but, as well, compensation for various major distortion factors (sources of errors) involved in this process. As presented, the emphasis is on quadratic curves since they are more common than others in machine vision. But, as a consequence of its general formulation, the method can be applied to higher-ordered curves as well.

In machine vision and computer vision, quadratic-curve-related situations (involving conic sections) occur in various forms and in various contexts. That quadratic curves are common and important in both fields is due to several factors: (1) many man-made objects are bounded by quadratic surfaces or have quadratic-curved edges; (2) quadratic curves or surfaces have been used as artificial landmarks in many machine-vision-related problems; (3) under both orthographic and perspective projections quadratic curves always map onto quadratic curves [1, 2]; (4) after first-order approximation (straight-line fitting), second-order (segmental or piecewise) approximation of curves is computationally cheapest and most common. Among the quadratic curves, the circle and its image (always an exact ellipse under either orthographic or perspective projections) are the most common. Thus, the focus of this paper will be on circular and elliptical curves. However, the method presented can be applied to other quadratic curves, as well, simply by modifying the global interpolation technique that is detailed for circles and ellipses in this paper.

Basically, we can classify quadratic-curve-related problems into three groups depending on the context in

which they occur: (a) pattern recognition and scene analysis, (b) machine-vision metrology, and (c) 3D location estimation problems in both direct and inverse forms. In all of these cases, parameters of quadratic curves must be estimated, either for the purpose of measurement (size comparison) in the 2D image plane, or for the more complex purpose of 3D orientation and position estimation in object space.

In scene analysis, the process of detection of ellipses as relatively abstract tokens or as confirmation items has been studied [3, 4]. In reconstruction or representation, conic sections have also been used for objects that are bounded by quadratic surfaces [5]. Approximation of noise-corrupted data in the image plane by quadratic curves has been widely used as a solution to various machine-vision problems. From a purely mathematical point of view, this problem has been addressed in a number of papers [6–8]. As well, the same problem has been addressed in the applied literature: for example, in dentistry, for estimation of the dental arch form [9], and in biology, for automatic chromosome analysis [10]. In all the above situations, only a *global* interpolation technique has been used to compensate for various sources of error.

In the case of quality control and inspection in an industrial environment, estimation of circular arc radius and center coordinates is a common problem [11, 12]. In this context, a high degree of accuracy in the estimated parameters is essential. Again, only a *global* interpolation technique has been used, and the effect of various existing sources of error has not been addressed explicitly.

Artificial (as well as natural) circular and spherical landmarks have been used in various pose-estimation problems: for 3D position (or location) estimation of a mobile robot [13–18], for 3D location estimation of objects [19, 20], and for human-arm-motion studies [21]. Circular shapes have been used extensively for defining calibration points for camera-calibration purposes [22]. Other quadratic curves have also been proposed for camera pose estimation [23]. For high precision assembly tasks using visual servoing, natural circular shapes have been used [24]. For precise positioning of surface-mount components, circular landmarks are used as well [25]. Though, within this class of problems, various levels of accuracy are required, the required level is generally high.

In the process of transformation of a curve in object space to another in computer-image space, the signal goes through several opto-electronic processes, by each of which it is distorted, either linearly or non-linearly. Accordingly, the accuracy of estimated parameters depends not only on an accurate global interpolation, but, as well, on compensation for major sources of error. These major sources of error can be divided into three

groups: errors due to quantization of light intensity; errors due to opto-electronic factors; and errors due to spatial quantization or other types of spatial errors (e.g., scattered data). These factors have been addressed separately in various papers; that is, each has been considered independently of the others. For example, several mathematical and statistical treatments of the spatial quantization problem have been published [26–29]. As well, the quantization of light intensity has been studied by several researchers [30–33].

In this paper, we address the problem in its *totality*, and present a general practical method for dealing with it. Thus, for example, we can handle the 3D location estimation of a mobile robot using a circular landmark, in which the image is an elliptical shape. For this problem, absolute accurate estimation of all five basic parameters in the image plane is essential. This problem, in its *totality*, encompasses all of the issues discussed above. To provide practical sequential procedures for the solution of such problems is our objective.

In Section 2 of this paper, the main sources of error that cause distortion in the shape of a curve are presented, and methods for their compensation are formulated. In Section 3, a new sub-pixel edge detection operator based on a circular approximation of the boundary of an object inside the detection area, and the sample-moment-preserving transform (SMPT), is discussed and its performance is compared with the one based on linear approximation. In Section 4, a new method for the determination of an optimal quadratic-curve fit (global interpolation) to a set of input edge points, is presented. For this purpose, an error function, based on a new geometrical interpretation of minimum-squares error (MSE) fit of quadratic functions, is defined; an objective and independent measure for “goodness” of various fits is formulated; as well, performance of the method compared to ones previously developed is discussed. In Section 5, experimental results for a set of circles located in 3D object space are presented; as well, the level of accuracy obtained using the sequential distortion-compensation procedure formulated in this paper is discussed. In the final section, Section 6, conclusions are presented.

2. MAIN FACTORS CAUSING DISTORTION IN 2D SHAPES

In general, the image of a nominal curvilinear shape acquired by a CCD camera is distorted by several factors. Thus, the image must go through several compensation processes in order to provide an accurate estimation of the shape’s parameters. This sequential compensation procedure is as follows:

(a) *Sub-pixel edge detection*: From a grey-level image of a curve, and all the available information it contains, one must detect the curve edge with subpixel accuracy.

Note that in practice one is faced with both quantization of light intensity and spatial quantization, as well as the ambiguity produced by ambient lighting variation around the edge of the actual curve; thus it is generally impossible to identify edge points precisely by mere thresholding. As a result, a new sub-pixel edge detector based on the principle of the sample-moment-preserving transform (SMPT) has been developed for accurate edge detection. It is presented in Section 3.

(b) *Transformation of computer-image coordinates to real image coordinates:* Computer-image coordinates are expressed in terms of pixel units. Our goal is to define edge points in terms of absolute length units (that is, in mm), and also to compensate for the timing mismatches which occur between image-acquisition hardware and camera scanning hardware (or even imprecision in the timing of the TV scan itself). For an uncertainty factor S_x , used to represent the mismatch, the following transformation is applied [34]:

$$\begin{aligned} X_d &= \frac{d'_x}{S_x} (X_f - C_x) \\ Y_d &= d_y (Y_f - C_y). \end{aligned} \quad (2.1)$$

Here (X_d, Y_d) is the (lens-) distorted real image coordinate, (X_f, Y_f) is the computer-image coordinate with sub-pixel accuracy, (C_x, C_y) is the computer-image coordinate of the center of the computer frame memory, S_x is the uncertainty image scale factor, and d_y is the center-to-center distance between adjacent CCD sensor elements in the Y direction. Furthermore, d'_x is defined as

$$d'_x = d_x \frac{N_{cx}}{N_{fx}}, \quad (2.2)$$

where d_x is the center-to-center distance between adjacent CCD sensor elements in the X direction, N_{cx} is the number of sensor elements in the X direction, and N_{fx} is the number of pixels in a line as sampled by the computer. S_x , C_x , and C_y are estimated by accurate camera calibration, and the values for the other parameters (d_x , d_y , N_{cx} , and N_{fx}) are supplied by manufacturers of CCD cameras and digitizer boards.

(c) *Lens radial distortion compensation:* The transformation between undistorted true-image coordinates (X_u, Y_u) , and distorted real-image coordinates (X_d, Y_d) can be defined as [34]

$$\begin{aligned} X_u &= X_d(1 + K_d r^2) \\ Y_u &= Y_d(1 + K_d r^2), \end{aligned} \quad (2.3)$$

where,

$$r = \sqrt{X_d^2 + Y_d^2}$$

and K_d , the radial distortion factor, is determined through accurate camera calibration.

(d) *Global interpolation:* Based on a set of true image coordinates (X_u, Y_u) , one must estimate the parameters of the imaged curve. Herein, the objective is to minimize the effect of spatial *scatteredness* on the parameter estimates and achieve an *accurate global* fit. In Section 4, this problem is discussed in detail for quadratic curves. Therein, a new error function is formulated for the optimal estimation of the parameters of a curve. Furthermore, based on an objective performance measure introduced there, this error function is compared to other error functions previously developed.

3. SUB-PIXEL EDGE DETECTION

As already noted, the image of an actual curve acquired by a CCD camera is distorted due to several factors. Thus, the image must be compensated by several processes in order to obtain an accurate estimation of the curve's parameters. One of the major distortion factors is the spatial and light-intensity quantization (digitization) process [27–29]. Another major factor originates in the actions of conventional edge-detection operators. It can also be noted that in practice shadows form around the edges of an object in an image—for example, the camera calibration plate (see Fig. 1). Thus, it is very difficult to identify edge points precisely by mere global thresholding. One way to deal with this type of distortion is through the use of sub-pixel edge detection [30, 31, 35, 36]. The objective of our work in this section (3), is to improve the overall performance of the edge-detection procedure by achieving a reasonable trade-off between accuracy and computational cost.

Section 3.1 of this paper provides an overview of the sample-moment-preserving transforms (SMPT) used in the development of a class of sub-pixel edge detectors. The approach using a linear border curve is reviewed in Section 3.2. Section 3.3 presents the newly developed sub-pixel edge detector based on a circular approximation of the border curve. Experimental results and a comparative study of the performance of the two edge operators (linear and circular) are presented in Section 3.4.

3.1. Edge Detection Using the Sample-Moment-Preserving Transform

The sample-moment-preserving transform (SMPT) has been implemented as a restorative transform in a number of applications such as edge detection [30, 31], image sharpening [37], thresholding [38], clustering [39], pattern matching [40], and corner detection [41]. SMPT-based edge detectors can be classified as belonging to the group of parametric edge detectors [42]. In principle, their operation consist of fitting a pre-defined edge model to the empirically-obtained gray-level-coded intensity data

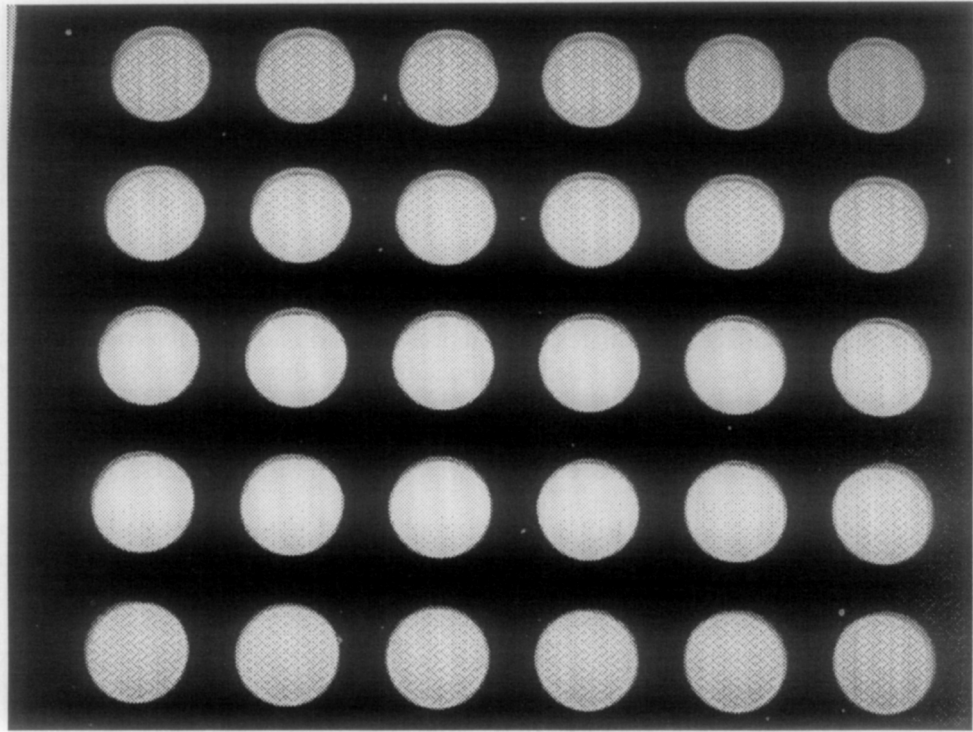


FIG. 1. A camera calibration scene.

$I(x, y)$, defined within a circular detection area. The edge detector accepts as input the gray-level-coded intensity data of a set of 69 pixels each having a weighting coefficient w_j , chosen so that the detection area will best approximate a circle with radius r of 4.5 pixel units. According to the model, the edge element is considered to occur on the border of two adjacent regions A_1 and A_2 . These regions, with areas a_1 and a_2 respectively, have constant intensities h_1 and h_2 with relative frequencies of occurrence p_1 and p_2 , where $p_1 + p_2 = 1$ (Fig. 2). The

edge detector is defined so that, when applied to the input intensity data $I(x, y)$ within the detection circle, it will produce an edge element determined by the values of triples (a_1, h_1, p_1) and (a_2, h_2, p_2) with the first three sample moments M_i of $I(x, y)$ being preserved [30, 31].

The values of the parameters of the edge model are computed by solving the equations of the SMPT:

$$p_1 h_1^i + p_2 h_2^i = M_i = \sum_{j=1}^{69} w_j I^i(x, y) \quad i = 1, 2, 3. \quad (3.1)$$

The probability-distribution function of the computed intensities of the edge model determines the edge location with sub-pixel precision.

Regions A_1 and A_2 of the edge model are separated by a border curve described by an equation in the XY coordinate system of the detection circle. The values of the parameters of the equation are derived based on an a priori assumption regarding the geometry of the border curve.

The SMPT-based edge detectors perform well in the presence of noise, as documented in [31] both analytically and experimentally.

3.2. Linear Border Curve

Tabatabai and Mitchell [30] assume that the border curve is nearly straight locally and derive a line equation

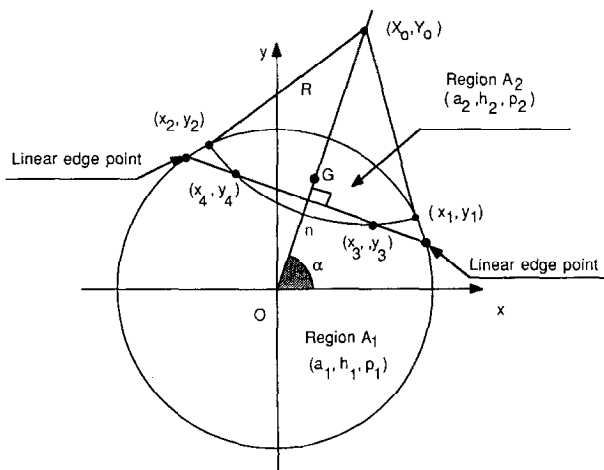


FIG. 2. Parameters of the edge model.

to approximate the border curve for their linear-edge detector. The linear border segment is described by its normal equation with respect to the coordinate system of the detection circle (Fig. 2):

$$\begin{aligned} x \cos \alpha + y \sin \alpha &= -l \quad \text{if } p_1 \leq p_2 \\ x \cos \alpha + y \sin \alpha &= l \quad \text{otherwise.} \end{aligned} \quad (3.2)$$

The parameters $\sin \alpha$ and $\cos \alpha$ are derived by using the center of gravity G of $I(x, y)$. These coordinates, with respect to the coordinate system of the detection circle, are defined as

$$\begin{aligned} G_x &= \frac{h_1 \int_{A_1} \int x \, dx \, dy + h_2 \int_{A_2} \int x \, dx \, dy}{h_1 \int_{A_1} \int dx \, dy + h_2 \int_{A_2} \int dx \, dy} = \frac{\sum_{j=1}^{69} x_j w_j I_j}{\sum_{j=1}^{69} I_j w_j} \\ G_y &= \frac{h_1 \int_{A_1} \int y \, dx \, dy + h_2 \int_{A_2} \int y \, dx \, dy}{h_1 \int_{A_1} \int dx \, dy + h_2 \int_{A_2} \int dx \, dy} = \frac{\sum_{j=1}^{69} y_j w_j I_j}{\sum_{j=1}^{69} I_j w_j}, \end{aligned} \quad (3.3)$$

where (x_j, y_j) are the coordinates of the center of the j th pixel with gray-scale value I_j and weighting coefficient w_j .

The angle α defines the inclination of the normal n from the origin of the detection circle to the linear boundary segment, and can be obtained from the following expressions:

$$\begin{aligned} \sin \alpha &= \frac{G_y}{\sqrt{G_x^2 + G_y^2}} \\ \cos \alpha &= \frac{G_x}{\sqrt{G_x^2 + G_y^2}}. \end{aligned} \quad (3.4)$$

The value of the normal distance l is derived by computing the area enclosed between the linear boundary segment and the circle:

$$a_2 = p_2 \pi r^2 = \int_{A_2} \int dx \, dy. \quad (3.5)$$

The solution of the integral leads to one of the following equations for the unknown l :

$$r^2 \arcsin \left(\frac{\sqrt{r^2 - l^2}}{r} \right) - l \sqrt{r^2 - l^2} - a_2 = 0 \quad \text{if } p_1 \geq p_2$$

$$0.5 \pi r^2 - l \sqrt{r^2 - l^2} - r^2 \arcsin \left(\frac{l}{r} \right) - a_2 = 0$$

otherwise.

$$(3.6)$$

3.3. Circular-Arc Border Curve

Approximating the border curve by higher-order planar segments requires the solution of a set of non-linear equations. Chen and Tsai have developed such a curve-edge detector which approximates the border curve by a parabolic segment and assumes a line-edge profile [37]. The values of the three parameters of a parabola are derived by numerically solving a system of three non-linear equations.

In the context of our research, the circular-arc approximation within the detection circle was considered to be a more accurate local approximation of the boundary of quadratic curves. The edge profile is assumed to be a step-edge profile. The SMPT-based circular-arc edge detector presented in this paper is defined so that, when applied to the empirically obtained gray-level-coded intensity data $I(x, y)$, it locates a set of edge points lying on a circular arc approximating the border curve within the detection circle.

As noted, the border curve within the detection circle is assumed to be approximated by a circular arc (Fig. 2) described by the following equation

$$(x - X_0)^2 + (y - Y_0)^2 = R^2 \quad \text{for } (x, y): x^2 + y^2 \leq r^2, \quad (3.7)$$

where R is the radius of the approximating circle and (X_0, Y_0) are the coordinates of its center with respect to the coordinate system of the detection circle.

As indicated in Fig. 2, candidates for these edge points appear to be the intersection points (x_3, y_3) and (x_4, y_4) of the approximating circle and the linear segment produced by a linear edge detector. A specific geometric relationship between the linear and the circular approximations of the border curve will be used to derive the equations for the coordinates of points (x_3, y_3) and (x_4, y_4) .

If the detection circle is rotated counterclockwise with respect to the origin through an angle of $(0.5\pi - \alpha)$, then the normal n coincides with the Y -axis (Fig. 3). Let X'_0 and Y'_0 denote the coordinates of the center of the approximating circle. The coordinates of the rotated intersection point (x'_3, y'_3) (and (x'_4, y'_4) as well) is related to the original intersection point through the following equations:

$$x'_3 = x_3 \sin \alpha - y_3 \cos \alpha$$

$$y'_3 = l = x_3 \cos \alpha + y_3 \sin \alpha. \quad (3.8)$$

The area a_2 of region A_2 , bounded by the detection circle and the rotated approximating circle is defined as follows:

$$a_2 = p_2 r^2 \pi = 2 \int_0^{x'_1} \int_{(Y'_0 - (R^2 - x^2)^{1/2})}^{(r^2 - l^2)^{1/2}} dy dx. \quad (3.9)$$

The following equations for the unknown x'_3 can be derived solving the double integral in Eq. (3.9):

$$r^2 \arcsin\left(\frac{x'_1}{r}\right) + R^2 \arcsin\left(\frac{x'_1}{R}\right) - x'_1 Y'_0 - a_2 = 0$$

if $p_1 \geq p_2$

$$0.5\pi r^2 + r^2 \arccos\left(\frac{x'_1}{r}\right) + R^2 \arcsin\left(\frac{x'_1}{R}\right)$$

$$- x'_1 Y'_0 - a_2 = 0 \quad \text{otherwise}$$

$$Y'_0 = l + \sqrt{R^2 - x'^2_3}$$

$$x'_1 = \left(r^2 - \left(\frac{r^2 - l^2 + 2lY'_0 - x'^2_3}{2Y'_0} \right)^2 \right)^{1/2}. \quad (3.10)$$

Due to the symmetry with respect to the Y -axis in Fig. 3, and since the linear segment and the circular arc enclose regions from the detection areas with equal areas (parameter a_2 of the edge model), the areas Ω_1 and Ω_2 are equal. This provides the incentive to conjecture that the relative position of point (x'_3, y'_3) on the linear segment is a very “weak” function of R . Let K denote the relative position of point (x'_3, y'_3) , that is,

$$K = \frac{x'_3}{\sqrt{r^2 - l^2}}. \quad (3.11)$$

The above conjecture was checked by solving Eqs. (3.10) for the unknown x'_3 with varying l within the interval $(-4.5, 4.5)$ pixel units with R ranging from 4.5 to 300 pixel units. For each x'_3 the corresponding value of K was

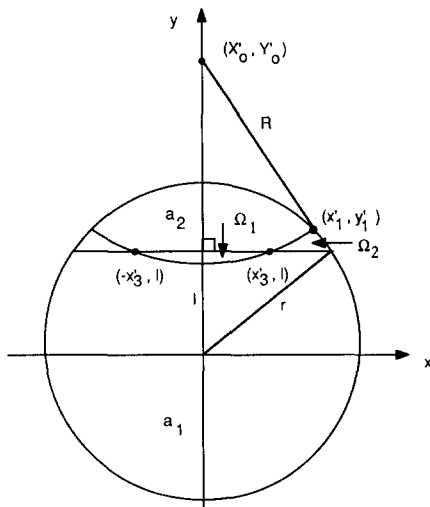


FIG. 3. A detection circle rotated through an angle $(0.5\pi - \alpha)$.

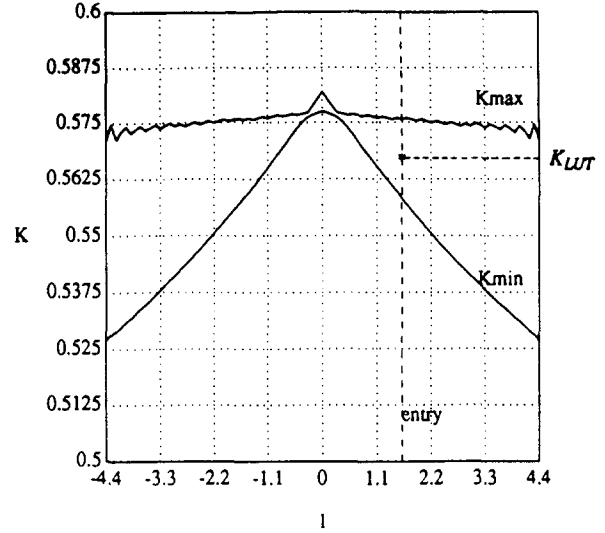


FIG. 4. The envelope for the values of K .

computed. The maximum and minimum values of K for each l are plotted in Fig. 4. The curves for K_{min} and K_{max} delimit a narrow butterfly-shape envelope for the relative position K of point (x'_3, y'_3) (and x'_4, y'_4) as well. The width of the envelope varies from 0.0011 to 0.046 depending on l .

This specific geometric relationship between the linear and the circular approximation of the boundary curve within the detection circle suggests that it is possible to design an arc-edge detector as a cascade of a linear edge detector and a look-up table (LUT). The mean values of K for each l with resolution 0.1 pixel units has been used to create a LUT.

Assuming that the values of the parameters $\sin \alpha$, $\cos \alpha$, and l have been computed by a linear edge detector, and the value of K has been obtained from the LUT, then the coordinates of the edge points (x_3, y_3) and (x_4, y_4) can be obtained from Eqs. (3.8) and (3.11):

$$\begin{aligned} x_3 &= l \cos \alpha + K \sin \alpha \sqrt{r^2 - l^2} \\ y_3 &= l \sin \alpha - K \cos \alpha \sqrt{r^2 - l^2} \\ x_4 &= l \cos \alpha - K \sin \alpha \sqrt{r^2 - l^2} \\ y_4 &= l \sin \alpha + K \cos \alpha \sqrt{r^2 - l^2}. \end{aligned} \quad (3.12)$$

The arc-edge detector discussed above has been applied to the image obtained from the camera-calibration scene (Fig. 1). In the implementation strategy, the image is first segmented and the boundaries of those regions containing each of the objects of the scene are chain-coded [43]. The resulting chain-code description (Fig. 5) is used to define a path on which the edge detector is applied. The

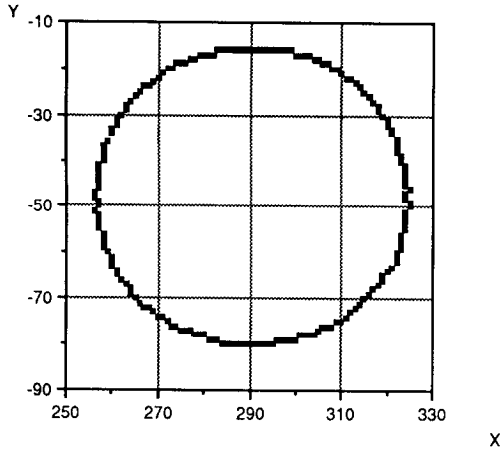


FIG. 5. A path for the circular-arc-edge detector.

output of the arc-edge detector applied to the third object in the left upper corner of the camera-calibration scene (Fig. 1) is shown on Fig. 6.

It should be noted that the use of a look-up table introduces a certain computational error. The absolute error Δa of the LUT is defined as a "difference between areas" of the detection circle, which the linear segment and the circular arc enclose. For each l , the absolute error Δa is a function of R , which can be computed through the following procedure:

- fix a value of l (less than 4.5 pixel units);
- compute the area a_{2l} bounded between the linear segment and the detection circle by using Eq. (3.6);
- use l as an entry to the LUT and obtain the value of K ;
- compute the coordinates of the point $(x'_3, y'_3 = l)$ by using Eq. (3.12);
- select a value for the variable R ;
- compute the area a_{2r} bounded between the circular arc and the detection circle by applying Eqs. (3.10);
- then, by definition, compute $\Delta a = a_{2r} - a_{2l}$.

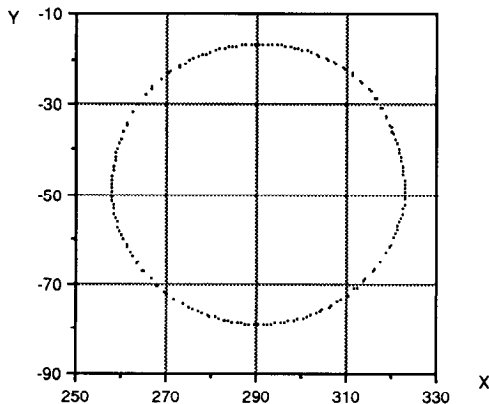


FIG. 6. An edge map of an elliptical-shape boundary.

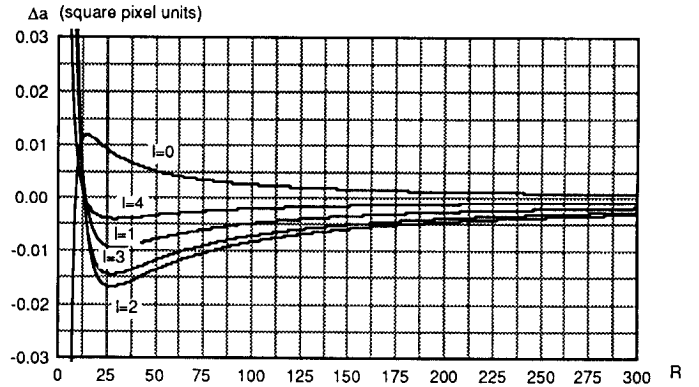


FIG. 7. Look-up table error.

A family of curves presenting Δa as a function of R is shown in Fig. 7. The maximum value of the absolute error for each l does not exceed 0.017 square pixel units for R greater than 10 pixel units.

3.4. The Comparative Performance of the New Sub-Pixel Edge Detector

Both edge operators (based respectively on linear and circular approximations of edge borders) were applied to all the elliptical shape boundaries in the image of the calibration plate (Fig. 1). The results comprise two sets of 2D sub-pixel coordinates of edge points. It should be noted that in the case of the linear edge detector, the intersection points of the linear segment and the detection circle have been taken as edge points (Fig. 2). The performance of the edge detector was evaluated through the estimation of the the total deviation of the set of detected sub-pixel edge points from the optimal elliptical fit in MSE sense. An error measure was defined as "the sum of the normal distances of all the edge points to the optimal ellipse."

Based on the experimental results obtained for the amount of the error measure, the details of which have been published elsewhere [32], the circular edge operator has a better (from the accuracy point of view) performance than the linear edge operator. The average deviation and the standard deviation of the circular-arc edge points from the elliptical fit (0.136 and 0.174 respectively) are almost three times less than those detected by the linear edge operator. This is expected due to the nature of the boundary approximation within the detection circle.

4. PARAMETER ESTIMATION OF QUADRATIC CURVES

As was indicated earlier, a circle and its image (an ellipse) are the most common quadratic curves in machine vision. Thus, in the following sections, parameter estimation of an elliptical shape is discussed, though, the overall methodology is applicable to other quadratic curves as well.

4.1. Problem Statement

As noted earlier, the need for the accurate estimation of the basic parameters of an elliptical shape arises in various machine-vision-related situations. In this section, we briefly review techniques which have been proposed by various research groups, and formulate the problem to be addressed.

One method for dealing with the elliptical-estimation problem is based on the use of *optimization* techniques. From a purely mathematical point of view, the problem of fitting a conic or a conic section to a set of data has been addressed in various papers [6, 7]. The same problem is also addressed in the applied literature: in dentistry, for the estimation of dental arch form [9]; in biology, for automatic chromosome analysis [10]; in the quality control of manufactured parts, for the estimation of an arc center and its radius [11–12]; in vision-based assembly, for polygonal and elliptical approximation of mechanical parts [44]; in object recognition, for detecting cylindrical parts and their orientation [19]; and, in pattern recognition and scene analysis, for the reconstruction problem [5, 8].

Other methods for dealing with the same problem have been investigated: using the Hough transformation for detection of curves (e.g., circles) [45]; using a modified Hough transformation for detecting ellipses [46]; decomposing the five-dimensional Hough transformation space into three sub-spaces based on the edge-vector-field properties of ellipses [47]; and estimating the parameters of an ellipse by combining transformation, projection, and optimum approximation techniques [3].

Most of the papers referred to above are concerned more with ellipse *detection*, while providing only a rough estimate of parameters. So, generally speaking, accuracy is not an important aspect in their development. Even those who actually seek accurate estimation of ellipse parameters confine themselves to finding the “best” fit to a final set of data points. As we have already shown in Section 2, for accurate estimation of the parameters, one must consider other factors as well.

It is important to emphasize that the quality of input data has a major impact on the accuracy of parameter estimation. No matter how good the fit may be, when the accuracy of input data is low, accurate estimation of parameters is not possible (the poisoned-point problem). The problem is one of quantization error (in both the light-intensity and spatial domains). This important factors has been addressed in a number of studies [27, 29]. Subpixel edge detection is closely related to this data-accuracy problem and was addressed in Section 3.

In this section, it will be assumed that the input data have a high degree of accuracy, as if obtained through subpixel edge detection and following the removal of quantization error. This assumption leads to the follow-

ing definition of the problem to be solved: “Given a set of 2D-image coordinates of edge points of an elliptical shape, it is required to determine the best ellipse fitting those points and subsequently estimate its five basic parameters: location, (X_0, Y_0) (ellipse center), orientation, Θ_A (the angle between the major axis of the ellipse and the X -axis of the computer-image frame), and shape, A, B (major and minor radii).”

4.2. Parameter Estimation

There are several different methods for the solution of this problem, depending on the number of parameters that must be estimated, their expected level of accuracy, and the acceptable computational cost. In this paper, we present three different methods, the experimental data obtained for each, and a discussion on their comparative performance.

Estimation of the five parameters of an ellipse based on a set of 2D coordinates can be achieved by defining an error function and then minimizing it. However, the accuracy and cost of the estimation process depend on the geometrical nature of the error function, whether this function is linear or non-linear, as well as on its form.

4.2.1. The Error Function J_1 and Its Geometrical Nature

Let

$$Q(X, Y) = aX^2 + bXY + cY^2 + dX + eY + f = 0 \quad (4.1)$$

be the general equation of an ellipse. Let

$$(X_i, Y_i) \quad i = 1, N \quad (4.2)$$

be a set of points to be fitted to an elliptical shape. Then, if one considers the value of $Q(X, Y)$ at a given point (X_i, Y_i) , the quantity $Q(X_i, Y_i)$ vanishes if the point is on the ellipse, it is negative if the point is inside, and it is positive if the point is outside the ellipse. Accordingly, one technique for fitting an elliptical shape to a given set of N points would be to use the minimum-squares error criterion which minimizes the error function

$$J_0 = \sum_{i=1}^N [Q(X_i, Y_i)]^2. \quad (4.3)$$

Thus, the objective is to determine a parameter vector $W^T = (a, b, c, d, e, f)$. Although, this error function has been used by different researchers, each of whom has used different constraints and solution methods, most have not discussed the geometrical nature of the optimi-

zation process based on it. An exception is Cooper and Yalabik [8] who considered this aspect of the problem for an elliptical shape while assuming f to be equal to -1 . As well, later, Bookstein [7] discussed it for the general case (Eq. 4.1) and showed the geometry of error-of-fit for *all* conic sections. With reference to Fig. 8, he has proved that

$$Q(X_i, Y_i) \propto \left[\frac{d_i}{d'_i} \left(\frac{d_i}{d'_i} + 2 \right) \right], \quad (4.4)$$

where (d_i/d'_i) is the ratio of the distances $(P_iP'_i)$ and $(O'P'_i)$, P_i is an edge point, O' is the center of the optimal ellipse, and P'_i is a boundary point of the optimal ellipse along the ray P_iO' . Since d_i is a maximum in the direction of the ellipse's major axis, and a minimum in the direction of the ellipse's minor axis, it can be seen that if two data points are equidistant from the ellipse, with one lying along the major axis and the other along the minor axis, then, the contribution to (4.3) of the data point lying along the minor axis will be greater.

In this paper, we analyze a solution method [5] which is based on the constraint $f \equiv 1$ (implying normalization with respect to f), for which Eq. (4.1) becomes

$$Q(X, Y) = aX^2 + bXY + cY^2 + dX + eY + 1. \quad (4.5)$$

Using the minimum-squares error criterion, the error function is then defined as

$$J_1 = \sum_{i=1}^N [Q(X_i, Y_i)]^2_{f=1}. \quad (4.6)$$

This method leads to a set of linear equations, for which the optimization process is non-iterative and therefore computationally fast. However, due to the geometrical nature of the error function, the contribution of data points is not uniform, a fact which affects the accuracy of the parameter estimates.

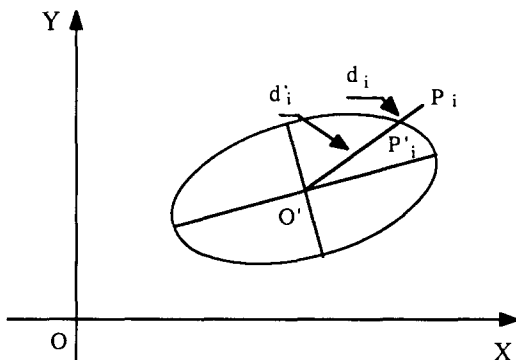


FIG. 8. Distances d_i and d'_i of an ellipse.

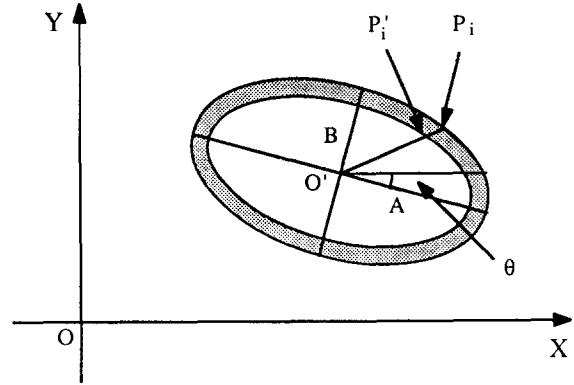


FIG. 9. The area difference of two concentric ellipses.

4.2.2. A New Geometrical Interpretation for J_1

Although researchers mentioned above [7, 8] have discussed the geometrical nature of the MSE function for quadratic curves and Cooper and Yalabik [8] have even indicated the non-uniformity of the contribution of the data points to the MSE function, they did not suggest any solution for the problem this produces. Thus, it is of interest to define an error function such that the contribution of the data points to the error function would be uniform. In order to achieve this, one must attempt first to clarify the geometrical nature of the error function J_1 defined in (4.6), and then to normalize the contributions of data points to it.

Let $(X_i, Y_i)(i = 1, N)$ be a set of data points, and let the optimal parameters of the ellipse be (A, B, Θ, X_0, Y_0) . Furthermore, let $(A', B', \Theta, X_0, Y_0)$ be the parameters of the ellipse that passes through the data point (X_i, Y_i) . The two ellipses are concentric and have the same eccentricity and the same orientation (Fig. 9). An error can be now defined as the difference between the areas of two ellipses,

$$e_i = S - S'_i. \quad (4.7)$$

In order to calculate S'_i , first consider a line that passes through a data point $P_i(X_i, Y_i)$ and the center $O'(X_0, Y_0)$; the intersection point of this line with the optimal ellipse is $P'_i(X'_i, Y'_i)$. By defining $d_i = P'_iO'$, $d'_i = P_iO'$, and $\delta_i = d'_i - d_i$, the following relation can be derived, based on the similarity of two ellipses:

$$e_i = \pi(AB) \left(1 - \frac{d_i'^2}{d_i^2} \right). \quad (4.8)$$

Using the definition of δ_i , (4.8) can be re-written in the form

$$e_i = \pi(AB) \left[\frac{\delta_i}{d_i} \left(\frac{\delta_i}{d_i} + 2 \right) \right]. \quad (4.9)$$

Comparison of the two relations, (4.4) and (4.9), shows that they both represent the same geometrical quantity. To further clarify this issue, an explicit expression for the term $(1 - d_i^2/d_i^2)$ in (4.8) can be derived as

$$1 - \frac{d_i'^2}{d_i^2} = 1 - \frac{[(X_i - X_0)\cos \Theta + (Y_i' - Y_0)\sin \Theta]^2}{A^2} - \frac{[-(X_i' - X_0)\sin \Theta + (Y_i - Y_0)\cos \Theta]^2}{B^2}, \tag{4.10}$$

where (X_i', Y_i') are the coordinates of point P_i' . The expression on the right hand side of (4.10) is the equation of an ellipse when written explicitly in terms of its five parameters. This expression can be written in the form that was given in (4.1) as

$$1 - \frac{d_i'^2}{d_i^2} = -(aX_i^2 + bX_iY_i + cY_i^2 + dX_i + eY_i + f), \tag{4.11}$$

where

$$\begin{aligned} a &= (A^2 \sin^2 \Theta + B^2 \cos^2 \Theta)/A^2B^2 \\ b &= 2(B^2 - A^2)\sin \Theta \cos \Theta/A^2B^2 \\ c &= (A^2 \cos^2 \Theta + B^2 \sin^2 \Theta)/A^2B^2 \\ d &= -2 \left(aX_0 + \frac{b}{2} Y_0 \right) \\ e &= -2 \left(\frac{b}{2} X_0 + cY_0 \right) \\ f &= (aX_0^2 + bX_0Y_0 + cY_0^2 - 1). \end{aligned}$$

Thus, one can conclude that if the constant term in the equation of an ellipse is normalized so that it is equal to F , defined as

$$F \equiv (aX_0^2 + bX_0Y_0 + cY_0^2 - 1), \tag{4.12}$$

the expression for the error defined by (4.8) can be written as

$$e_i = -\pi(AB)[Q(X_i, Y_i)]_{f=F}, \tag{4.13}$$

where $Q(X_i, Y_i)$ is the equation of an ellipse, in which the constant term is normalized with respect to F .

Based on (4.13), one can define an error function as

$$\begin{aligned} J_2 &= \sum_{i=1}^N \left[\frac{1}{\pi AB} (S - S_i') \right]^2 = \sum_{i=1}^N \left[\frac{e_i}{\pi AB} \right]^2 \\ &= \sum_{i=1}^N [Q(X_i, Y_i)]_{f=F}^2. \end{aligned} \tag{4.14}$$

The comparison of J_2 with J_1 defined by (4.6) shows that the only difference between the two is that in $J_1, f \equiv 1$, while in $J_2, f \equiv F$, which is just a constant multiplication factor. Thus, one can conclude that the two error functions are equivalent. However, in the process of deriving an expression for J_2 , a new and clearer geometrical interpretation of the error function J_1 is obtained. In fact, it has been shown that the optimization of this error function minimizes the error generated due to the difference in *area* as defined in (4.7). Based on this new interpretation of the error function, we can define a new error function with improved performance.

4.2.3. An Improved Error Function J_3

In order to improve the performance of the optimization based on the error function J_1 , the contribution of each data point to the error function should be normalized. This can be achieved by defining a weighting factor which is a function of the position of an individual data point. Let δ_i be the distance of a particular data point to the optimal ellipse (P_iP_i' in Fig. 9). Then the amount of error due to this data point is

$$e_1 = \pi AB \left(\frac{\delta_i^2 + 2d_i\delta_i}{d_i^2} \right). \tag{4.15}$$

If this point, with the same δ_i , was on the major axis of the optimal ellipse, the error would be

$$e_2 = \pi AB \left(\frac{\delta_i^2 + 2A\delta_i}{A^2} \right). \tag{4.16}$$

Using (4.15) and (4.16), the following weighting factor can be defined for a data point (X_i, Y_i)

$$w_i = \frac{e_2}{e_1} = \left(\frac{d_i}{A} \right) \left(\frac{1 + \delta_i/2A}{1 + \delta_i/2d_i} \right). \tag{4.17}$$

As δ_i is normally much smaller than d_i or A , (4.17) can be approximated as

$$w_i \approx \left(\frac{d_i}{A} \right) \left(1 + \frac{\delta_i}{2A} - \frac{\delta_i}{2d_i} \right) \approx \frac{d_i}{A}. \tag{4.18}$$

Based on the weighting factor defined above, the proposed new error function is defined as follows:

$$J_3 = \sum_{i=1}^N \left[w_i \frac{1}{\pi AB} (S - S_i') \right]^2 = \sum_{i=1}^N [w_i Q(X_i, Y_i)]_{f=F}^2. \tag{4.19}$$

Or, if we use the constraint $f \equiv 1$,

$$J_3 = \sum_{i=1}^N [w_i Q(X_i, Y_i)]_{f=1}^2. \tag{4.20}$$

In order to avoid an *iterative* process, the coefficient w_i must be first estimated for each data point. To achieve this, one must have an *initial* “optimal” ellipse from which δ_i and d_i can be estimated for each data point. For this purpose, the error function J_1 can be used. Thereafter, the optimization (minimization) of the error function J_3 would proceed by taking the first derivatives with respect to the five unknowns (a, b, c, d , and e) to yield a set of five linear equations with five unknowns, the solution of which is the vector $W^T = (a, b, c, d, e)$. The five parameters of the final optimal ellipse can then be estimated using the equations

$$\begin{aligned} X_0 &= \frac{2cd - be}{b^2 - 4ac}, \quad Y_0 = \frac{2ae - bd}{b^2 - 4ac}, \\ \Theta_A &= \text{atan} \left[\frac{(c - a) + \sqrt{(c - a)^2 + b^2}}{b} \right], \\ A^2 &= \left[\frac{2(1 - F_s)}{b^2 - 4ac} \right] [(c + a) + \sqrt{(c - a)^2 + b^2}], \\ B^2 &= \left[\frac{2(1 - F_s)}{b^2 - 4ac} \right] [(c + a) - \sqrt{(c - a)^2 + b^2}], \end{aligned} \quad (4.21)$$

where

$$F_s = \frac{bde - ae^2 - cd^2}{b^2 - 4ac}.$$

4.3. Error Function J_4

Another existing error function, based on distance measurements, which has been claimed to have a better performance than J_1 , is briefly reviewed in this section for its comparison with the newly proposed J_3 function. Nakagawa and Rosenfeld [44] proposed the distance measure

$$J_4 = \sum_{i=1}^N d_i, \quad (4.22)$$

where d_i is the distance $P_iP'_i$ as defined in Fig. 9 for the data point (X_i, Y_i) .

As can be deduced, the error function is non-linear; thus the optimization process must be iterative. Moreover, the form of the error function J_4 is such that, in each iteration for its estimation, the contribution of each individual data point must be evaluated separately. As a result, the optimization process based on the J_4 error function can be very costly.

A final point that should be mentioned here is concerned with the idea of defining an error function based on the normal distance of a data point to an ellipse. This is a special case of a more general problem which is referred to as “function fitting based on minimization of perpendicular deviations.” There is no general algorithm

for this type of problem [6]. Though, as defined, it would yield a best fit, this error function is highly involved, complex, and computationally expensive. The reason is the non-linearity of its error function and the corresponding requirement for an iterative process of optimization. More importantly, in each iteration for every single point, a fourth-order equation has to be solved in order to find the normal distance.

4.4. An Objective Measure for “Goodness” of Fit

In order to carry out a comparative study of the three error functions J_1, J_3 , and J_4 , an objective and independent measure of “goodness” of fit is highly desirable. In this section, such an objective measure is defined as “the sum of normal distances of all the data points to the optimal ellipse,” and a procedure for its evaluation is presented.

This measure can be obtained following the optimization process of each error function. However, first, the coordinates of the intersection point of a normal line which passes through a particular data point and the optimal ellipse must be determined.

Thus, the initial problem can be defined as follows: Given a point (X_i, Y_i) and an ellipse with parameters (A, B, Θ, X_0, Y_0) , find the normal line to the ellipse which passes through point (X_i, Y_i) . In order to simplify the estimation process and obtain more manageable equations, a transformation consisting of a translation and then a rotation will be applied to all the data points and the optimal ellipse, as follows:

$$\begin{aligned} X_{i1} &= X_i - X_0 \\ Y_{i1} &= Y_i - Y_0 \\ X_{is} &= X_{i1} \cos \Theta + Y_{i1} \sin \Theta \\ Y_{is} &= -X_{i1} \sin \Theta + Y_{i1} \cos \Theta. \end{aligned} \quad (4.23)$$

Following this, the transformed equation of the optimal ellipse can be written in the following form:

$$\frac{X^2}{A^2} + \frac{Y^2}{B^2} = 1. \quad (4.24)$$

Let $P(X_i, Y_i)$ be a data point, PP'' be the normal to the ellipse (Fig. 10), and the coordinates of point P'' be (X''_i, Y''_i) . Thus, if m_1 is the slope of the tangent line at point P'' , and m_2 is the slope of line PP'' , then one of the constraints on the coordinates of point P'' is:

$$m_1 m_2 = -1. \quad (4.25)$$

It can be shown that the first constraint on point P'' can be expressed as follows (using 4.25):

$$\left(\frac{Y''_i - Y_i}{X''_i - X_i} \right) \left(\frac{X''_i}{Y''_i} \right) = \frac{A^2}{B^2}. \quad (4.26)$$

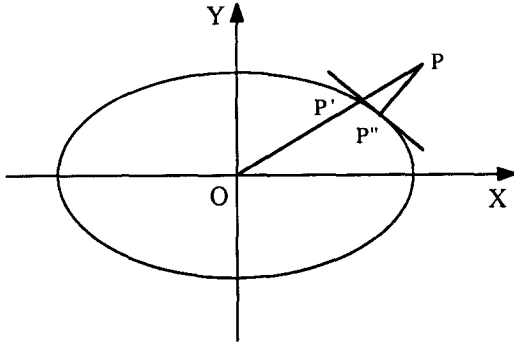


FIG. 10. Normal and "central" lines to an ellipse.

The second constraint on point P'' is that it must satisfy the equation of the optimal ellipse, i.e.,

$$\frac{X_i''^2}{A^2} + \frac{Y_i''^2}{B^2} = 1. \quad (4.27)$$

From (4.26), an expression for Y_i'' can be determined. Substituting this expression into (4.27) and simplifying it, a quartic equation is obtained,

$$X_i''^4 + a_1 X_i''^3 + a_2 X_i''^2 + a_3 X_i'' + a_4 = 0, \quad (4.28)$$

where

$$a_1 = \left[2A^2 \left(1 - \frac{A^2}{B^2} \right) X_i \right] / a_5$$

$$a_2 = \left[A^2 Y_i^2 - A^2 B^2 \left(1 - \frac{A^2}{B^2} \right)^2 + \frac{A^4}{B^2} X_i^2 \right] / a_5$$

$$a_3 = \left[-2A^4 \left(1 - \frac{A^2}{B^2} \right) X_i \right] / a_5$$

$$a_4 = \left[-\left(\frac{A^6}{B^2} \right) X_i^2 \right] / a_5$$

$$a_5 = \left[B^2 \left(1 - \frac{A^2}{B^2} \right)^2 \right].$$

Equation (4.28) can have a maximum of four real solutions, corresponding to which there would be at most four points satisfying the two constraints. Correspondingly, it can be shown that a data point (X_i, Y_i) can have either two or four normals to an ellipse. Furthermore, it can be shown that one of the normals yields the minimum distance to an ellipse, and this normal is the one that we want to determine. To solve equation (4.28) the method of solution of a quartic equation based on the resolvent cubic equation can be employed [48].

Once the coordinates of point P'' have been estimated

for all data points, $\delta_i' = PP''$ can be calculated for each point. The "goodness" measure is then defined as

$$G = \sum_{i=1}^N \delta_i', \quad (4.29)$$

where an error function that yields a smaller value for G is a better fit.

4.5. The Comparative Performance of Error Function J_3

In this section we present just the results of the overall performance comparison without giving the details of the experimental data. The details of the experimental results obtained for various cases and the corresponding data analysis have been published elsewhere [49].

As was indicated earlier, if an error function is non-linear, the optimization process is generally an iterative one. For such a process, a "good" initial set of unknown parameter values can reduce the number of iterations substantially, and reduce the chances of reaching a local minimum due to the non-linearity in the optimization process. The use of the J_1 error function is proposed for establishing the initial values, since J_1 is linear, and the estimation process of the five ellipse parameters based on it is non-iterative. Using the results of the optimization of J_1 as a set of initial values, the other two error functions, J_3 and J_4 , can be optimized. The iterative optimization method used in this study is the downhill simplex method due to Nelder and Mead [50].

Two different cases were considered: a simulated ellipse and an imaged ellipse. For the first case, a "perfect" ellipse is generated using digitizer-board graphic commands, the boundary of which is digitized according to a mathematical procedure that minimizes the digitization error of a continuous boundary of an ellipse. In the second case, an "imperfect" ellipse image was used to simulate possible external distortions, such as the thresholding effect on a grey-level image. The shape of this ellipse is further distorted by its passage through the image-acquisition system (that is, the camera and the digitizer, for which all the distortion factors that were earlier-mentioned apply). Each case was tested under three different conditions: (1) all edge points were used, (2) sampled edge points were used—sampled in 5-pixel steps along the Y -axis, and (3) sampled edge points of only a segment (approximately one third) of the ellipse's boundary were used.

The experimental results showed that the performance of the proposed error function J_3 is better in accuracy than the other two if all the edge points are used, as is often the case. However, when the number of edge points is reduced, or when a partial ellipse is considered, the *total* performance of J_4 (indicated by the "goodness"

measure G) is better than that of J_3 (although they are very close), and J_3 is better than J_1 . However, a general problem with J_4 is the iterative nature of its optimization process, and the need for the estimation of the function value for each individual data point in each iteration; as a result, it is computationally very expensive. Thus, we can conclude that the new error function provides an acceptable trade-off between relatively high accuracy and relatively low computational cost.

5. EXPERIMENTAL RESULTS

For experimentation purposes, we have considered a 3D location estimation problem which requires a relatively high degree of accuracy in the estimated parameters. Furthermore, this problem has been chosen due to its importance in machine vision. The objective in this experiment is to estimate accurately the 3D orientation and 3D position of a set of circular features. First, in Section 5.1, the total process that is involved (seven steps) is briefly summarized. Subsequently, in Section 5.2, the experimental results of the total process are presented.

5.1. The Total Process Involved in 3D Location Estimation

Accurate estimation of the 3D location of a circular feature from an input grey-level image requires a set of processes to compensate for various types of distortion, as well as a general analytical solution method. In a real process, as opposed to a simulated one, various sources of noise affect the input image and thus distort it. The experimental results in this section report the total process of accurate estimation of the 3D location of a circular feature, which involves the application of the sequential distortion-compensation procedure developed in this paper and a general 3D analytical solution method (having no simplifying assumptions) for circular features which was previously derived [51]. For completeness, a brief review of the steps involved in the total process is presented below:

(1) *Camera calibration.* The camera is calibrated by applying the mono-view non-coplanar points technique [34], as a result of which the 3D location of the camera frame with respect to a pre-defined world frame of reference is estimated. Furthermore, the effective focal length of the camera, the radial distortion factor of the camera's lens, and the uncertainty scale factor for the x -axis (due to the timing mismatches which occur between image-acquisition hardware and camera scanning hardware) are also obtained.

(2) *Sub-pixel edge detection.* After an image of a circular feature is acquired, the new sub-pixel edge detector developed in this paper is applied, whose result is a set of

sub-pixel edge-points data. The sub-pixel edge detector compensates for quantization error and estimates the local boundary of a circular feature more reliably.

(3) *Coordinate transformation.* Computer-image coordinates are expressed in terms of pixel units. To define the edge-points in terms of units of absolute length (in mm), and also to compensate for timing mismatches, a set of transformations are applied. These are implemented by using the uncertainty factor estimated in step (1) and technical specifications of the camera's CCD chip and the digitizer board.

(4) *Lens-radial-distortion compensation.* The estimated lens-radial-distortion factor in step (1) is applied to all edge-points to compensate for lens radial distortion.

(5) *Global interpolation and elliptical-shape-parameter estimation.* The interpolation technique based on the optimization of the new error function developed in this paper is applied to accurately estimate the five basic parameters of an ellipse—the perspective projection of a circle onto the image plane.

(6) *Circular-feature 3D-orientation estimation.* Using the estimated effective focal length in step (1) and the estimated values for the five basic parameters of an ellipse found in step (5), and applying the analytical method developed in [51], the 3D orientation of the circular feature with respect to the camera frame is estimated.

(7) *Circular-feature 3D-position estimation.* Using the estimated orientation of a circular feature in step (6) and its known radius, and applying the analytical method developed in [51], the 3D position of the feature is estimated with respect to the camera frame. Applying the transformation from the camera frame to the world frame of reference, obtained in step (1), to the estimated 3D position of the circle yields the 3D position with respect to the world-reference frame.

5.2. Experimental Results for the Total Process

For experimentation on the total process, six co-planar circles arranged into two columns on the left and right sides of the plane were used. The plane of the circles, in an inclined orientation with respect to the camera image plane, was positioned so that the field of circles extended over the entire field of view. These conditions provided the most general camera-circular-feature configuration. Furthermore, in order to obtain a sharp image of all circles, this plane was located within the approximated existing depth-of-field of the camera [52].

The application of the above seven-step procedure to the six coplanar circles resulted in two sets of data, tabulated in Tables 1 and 2. Through camera calibration, the orientation angles of the normal to the circles' plane was estimated. These are referred to as "Reference Angles" in Table 1. The estimated orientation angles of each cir-

TABLE 1
Estimated Orientation Angles of the Surface Normals of a Set of Circular Features

Angles	α (degree)	β (degree)	γ (degree)
Reference angles	89.72	76.73	13.27
Circle #1	88.73	76.06	13.99
Circle #2	89.61	74.99	15.01
Circle #3	88.75	76.54	13.52
Circle #4	89.87	76.39	13.61
Circle #5	89.11	76.43	13.60
Circle #6	87.46	77.93	12.34
Average angles	88.92	76.39	13.68
Average deviations	0.80	0.34	0.41

Note. α , β , γ are the angles which the surface normal of a circle makes with the x , y , z axes of the camera frame, respectively.

cle's norm are also presented in this table. Note that since the circles were coplanar, they must have the same orientation angle. The average orientation angle is defined as the mean value of the orientation angles of the six circles, while the average deviation is defined as the absolute value of the difference between a reference angle and an average angle. The average deviations of the three orientation angles were determined as, 0.80, 0.34, and 0.41 degrees, respectively. As can be seen, the results show only a small error indicative of the good performance of the total process.

In Table 2, the results of the position-estimation process are presented. The coordinates, estimated with respect to the world-reference frame, are given under the column "Estimated." The exact 3D coordinates of the circles' centers are known a priori and are given in Table 2 under the column "Reference." The differences between the reference and the estimated coordinates of all the circles are calculated, and the means of these values are given under "Average Deviations." The results can be better appreciated when the size of the field of view

(275 mm by 200 mm) and the focused distance (864 mm) are taken into consideration. The 1.28 mm average error for the depth estimation in an approximately 864 mm focused distance is less than 1.5 parts in 1000 average accuracy. As a whole, both sets of results show the validity of the total process involved in the 3D-location estimation in general, and the applicability of the methods developed in this paper in particular.

6. CONCLUSIONS

In this paper, the problem of accurate parameter estimation of quadratic curves was addressed. It was shown that this depends on both an accurate global interpolation and compensation of major sources of errors. As a result, a sequential distortion-compensation procedure was formulated. Subsequently, a new sub-pixel edge detector was developed for accurate coordinate estimation of edge points from grey-level images. It was designed as a cascade of a linear-edge detector and a look-up table. Furthermore, its performance was compared to that of a linear sub-pixel edge detector. As well, for accurate global interpolation purposes, an error function was derived based on a new geometrical interpretation of minimum-squares error fit of quadratic functions. Using an independent and objective measure for "goodness" of fit, developed in this paper, the performance of this error function was compared with the two other error functions. For experimentation on the total process involved in the accurate-parameter-estimation process, a 3D-location estimation problem was considered. The objective was to accurately estimate the 3D orientation and the 3D position of a set of circular features from a grey-level image. The experimental results obtained showed the validity of the total process involved in the accurate 3D-location estimation in general, and the effectiveness of the sub-pixel edge detector and the global interpolation technique, both developed in this paper, in particular.

TABLE 2
Estimated Positions of a Set of Circular Features

Coordinates	x (mm)		y (mm)		z (mm)	
	Reference	Estimated	Reference	Estimated	Reference	Estimated
Circle #1	0.00	0.38	0.00	0.63	10.00	8.05
Circle #2	185.00	184.78	0.00	-0.03	10.00	11.01
Circle #3	0.00	0.24	37.00	37.27	10.00	9.31
Circle #4	185.00	184.64	37.00	37.43	10.00	9.15
Circle #5	0.00	0.26	74.00	74.34	10.00	8.92
Circle #6	0.00	0.46	148.00	148.60	10.00	7.92
Average deviations		0.32		0.38		1.28

Note. All the coordinates are with respect to the world reference frame.

ACKNOWLEDGMENT

This work was partially supported by the Manufacturing Research Corporation of Ontario (MRCO).

REFERENCES

1. D. Hilbert and S. Cohen-Vossen, *Geometry and the Imagination*, first German ed., 1932; first English ed., Chelsea New York, 1952.
2. R. M. Haralick, Y. H. Chu, L. T. Watson, and L. G. Shapiro, Matching wire frame objects from their two dimensional perspective projections, *Pattern Recognition* **17**, 1984, 607–619.
3. R. Wang, A. R. Hansen, and E. M. Riseman, Fast extraction of ellipses, in *Proceedings, 9th International Conference on Pattern Recognition, Vol. 1, 1988*, pp. 508–510.
4. H. C. Lee and K. S. Fu, 3-D shape from contour and selective conformation, *Comput. Vision Graphics Image Process.* **22**, 1983, 177–193.
5. A. Albano, Representation of digitized contours in terms of conic arcs and straight-line segments, *Comput. Graphics Image Process.* **3**, 1974, 23–33.
6. R. Gnanadesikan, *Methods for Statistical Data Analysis of Multivariate Observations*, Wiley, New York, 1977.
7. F. L. Bookstein, Fitting conic sections to scattered data, *Comput. Graphics Image Process.* **9**, 1979, 59–71.
8. D. B. Cooper and N. Yalabik, On the computational cost of approximating and recognizing noise-perturbed straight lines and quadratic arcs in the plane, *IEEE Trans. Comput.* **C-25**, 1976, 1020–1032.
9. R. H. Biggerstaff, Three variations in dental arch form estimated by a quadratic equation, *Dent. Res.* **51**, 1972, 1509.
10. K. A. Paton, Conic sections in automatic chromosome analysis, *Mach. Intelligence* **5**, 1970, 411–434.
11. U. M. Landau, Estimation of a circular arc center and its radius, *Comput. Vision Graphics Image Process.* **38**, 1987, 317–326.
12. S. M. Thomas and Y. T. Chan, A simple approach for the estimation of circular arc center and its radius, *Comput. Vision Graphics Image Process.* **45**, 1989, 362–370.
13. M. J. Magee and J. K. Aggarwal, Determining the position of a robot using a single calibration object, in *IEEE Proceedings, International Conference on Robotics and Automation, Atlanta, GA, March 1984*, pp. 140–149.
14. M. R. Kabuka and A. E. Arenas, Position verification of a mobile robot using standard pattern, *IEEE J. Robotics Automation* **RA-3**, 1987, 505–516.
15. N. Olgac, Z. Gan, and B. E. Platin, 3-D recognition of object configurations by hybrid projection analysis using a single-camera image, in *Proceedings, 1st National Applied Mechanisms and Robotics Conference, Ohio, Nov. 1989*, Vol. I, pp. 1–6.
16. Y. Fainman, L. Feng, and Y. Koren, Estimation of absolute spatial position of mobile systems by hybrid opto-electronic processor, in *IEEE, Proceedings, International Conference on Systems, Man, and Cybernetics, Cambridge, MA, Nov. 1989*, Vol. II, pp. 651–657.
17. B. Hussain and M. R. Kabuka, Real-time system for accurate three-dimensional position determination and verification, *IEEE Trans. Robotics Automation* **6**, 1990, 31–43.
18. K. Mandel and N. A. Duffie, On-line compensation of mobile robot docking errors, *IEEE J. Robotics Automation* **RA-3**, 1987, 591–598.
19. T. Nagata, H. Tamura, and K. Ishihashi, Detection of an ellipse by use of a recursive least-square estimator, *J. Robotic Systems* **2**, 1985, 163–177.
20. R. Safaee-Rad, B. Benhabib, K. C. Smith and Z. Zhou, Pre-marking methods for 3D object recognition, in *IEEE Proceedings, International Conference on Systems, Man, and Cybernetics, Boston, MA, Nov. 1989*, Vol. II, pp. 592–595.
21. R. Safaee-Rad, E. Shwedyk, and A. O. Quanbury, Three dimensional measurement system for functional arm motion study, *Med. Biol. Engrg. Comput.* **28**, 1990, 569–573.
22. R. K. Lenz and R. Y. Tsai, Techniques for calibration of the scale factor and image center for high accuracy 3-D machine vision metrology, *IEEE Trans. Pattern Anal. Mach. Intelligence* **10**, 1988, 713–720.
23. R. M. Haralick, Solving camera parameters from the perspective projection of a parameterized curve, *Pattern Recognition* **17**, 1984, 637–645.
24. S. Baird, and M. Lurie, Precise robotic assembly using vision in the hand, in *Robot Sensors* (A. Pugh, Ed.), U.K., 1986.
25. N. S. Chang, Position measuring accuracy of loading surface mount components, *SPIE Proc., Automated Inspection Measurement* **730**, 1986, 151–155.
26. F. C. A. Groen and P. W. Verbeek, Freeman-code probabilities of object boundary quantized contours, *Comput. Graphics Image Process.* **7**, 1978, 391–402.
27. B. Kamgar-Parsi and B. Kamgar-Parsi, "Evaluation of quantization error in computer vision, *IEEE Trans. Pattern Anal. Mach. Intelligence* **PAMI-11**, 1989, 929–940.
28. S. D. Blostein and T. S. Huang, Quantization errors in stereo triangulation, in *Proceedings, First International Conference on Computer Vision, June 1987*, pp. 325–334.
29. C.-S. Ho, Precision of digital vision systems, *IEEE Trans. Pattern Anal. Mach. Intelligence* **PAMI-5**, 1983, 593–601.
30. A. J. Tabatabai and O. R. Mitchell, Edge location to sub-pixel values in digital imagery, *IEEE Trans. Pattern Anal. Mach. Intelligence* **PAMI-6**, 1984, 188–201.
31. L.-H. Chen and W.-H. Tsai, Moment-preserving curve detection, *IEEE Trans. Systems Man, Cybernet.* **18**, 1988, 148–158.
32. I. Tchoukanov, R. Safaee-Rad, B. Benhabib, and K. C. Smith, Sub-pixel edge detection for accurate estimation of elliptical shape parameters, in *Proceedings, CSME Mechanical Engineering Forum 1990, Toronto, Ontario*, Vol. III, pp. 313–318.
33. Y.-S. Li, T. Y. Young, and J. A. Magerl, Subpixel edge detection and estimation with a microprocessor-controlled line scan camera, *IEEE Trans. Industrial Electron.* **35**, 1988, 105–112.
34. R. Y. Tsai, A versatile camera calibration technique for high-accuracy 3D machine vision metrology using off-the-shelf TV camera and lenses, *IEEE J. Robotics Automation* **RA-3**, 1987, 323–344.
35. E. M. Mikail, M. L. Akey, and O. R. Mitchell, Detection and sub-pixel location of photogrammetric targets in digital images, *Photogrammetria* **39**, 1984, 63–83.
36. A. Huertas and G. Medioni, Edge detection with sub-pixel precision, in *IEEE, Proceedings, The Third Workshop on Representation and Control, Michigan, Oct. 1985*, pp. 63–74.
37. L.-H. Chen and W.-H. Tsai, Moment-preserving-sharpening—A new approach to digital picture deblurring, *Comput. Vision Graphics Image Process.* **41**, 1988, 1–14.
38. W.-H. Tsai, Moment-preserving thresholding: A new approach, *Comput. Vision Graphics Image Process.* **29**, 1985, 377–393.
39. S.-T. Liu and W. Tsai, Moment-preserving corner detection, *Pattern Recognition* **23**, 1990, 441–460.

40. C. Chou and Y. Chen, Moment-preserving pattern matching, *Pattern Recognition* **23**, 1990, 461–474.
41. S.-T. Liu and W. Tsai, “Moment-preserving clustering, *Pattern Recognition* **22**, 1989, 433–447.
42. A. Rosenfeld, and A. C. Kak, *Digital Picture Processing*, Academic Press, New York, 1976.
43. H. Freeman, Computer processing of line drawing images, *Comput. Surveys* **6**, 1974, 57–98.
44. Y. Nakagawa and A. Rosenfeld, A note on polygonal and elliptical approximation of mechanical parts, *Pattern Recognition* **11**, 1979, 133–142.
45. R. O. Duda and P. E. Hart, Use of the Hough transformation to detect lines and curves in pictures, *Comm. ACM* **15**, 1972, 11–15.
46. S. Tsuji and F. Matsumoto, Detection of ellipses by a modified Hough transformation, *IEEE Trans. Comput.* **C-27**, 1978, 777–781.
47. H. Tsukune and K. Goto, Extracting elliptical figures from an edge vector field, in *IEEE, Proceedings, Conference on Computer Vision and Pattern Recognition, Jan 1983*, pp. 138–141.
48. W. H. Beyer, *Standard Mathematical Tables*, CRC Press, Florida, 1981.
49. R. Safaee-Rad, K. C. Smith, and B. Benhabib, Accurate estimation of elliptical shape parameters from a grey-level image, in *IEEE, Proceedings, International Conference on Pattern Recognition, Atlantic City, NJ, June 1990*, Vol. II, pp. 20–26.
50. J.A. Nelder and R. Mead, A simple method for function minimization, *Comput. J.* **7**, 1965, 308–313.
51. R. Safaee-Rad, K. C. Smith, B. Benhabib, and I. Tchoukanov, An analytical method for the 3D-location estimation of circular features for an active-vision system, in *IEEE, Proceedings, International Conference on Systems, Man, and Cybernetics, Los Angeles, Nov. 1990*, pp. 215–220.
52. R. A. Morton (Ed.), *Photography for the Scientist*, second ed., Academic Press, London, 1984.